HHS Public Access

Author manuscript

Mol Neurobiol. Author manuscript; available in PMC 2024 January 06.

Published in final edited form as:

Mol Neurobiol. 2023 February ; 60(2): 495–511. doi:10.1007/s12035-022-03082-0.

Deletion of Small GTPase H-Ras Rescues Memory Deficits and Reduces Amyloid Plaque-Associated Dendritic Spine Loss in Transgenic Alzheimer's Mice

Wenhui Qu[1,2], **Angela Jeong**[3,4], **Rui Zhong**[3], **Josslen S. Thieschafer**[3], **Andrea Gram**[3], **Ling Li**[1,3]

[1]Graduate Program in Neuroscience, University of Minnesota, Minneapolis, MN 55455, USA

[2]Present Address: Department of Pathology & Cell Biology, Vagelos College of Physicians and Surgeons, Columbia University Irving Medical Center, New York, NY 10032, USA

[3]Department of Experimental and Clinical Pharmacology, University of Minnesota, Minneapolis, MN 55455, USA

[4]Present Address: Division of Pharmacotherapy and Experimental Therapeutics, Eshelman School of Pharmacy, University of North Carolina, Chapel Hill, NC 27599, USA

Abstract

Alzheimer's disease (AD) is a fatal neurodegenerative disorder, affecting millions of lives without a cure. While the molecular mechanism of AD remains obscure, emerging evidence suggests that small GTPases, a group of GTP-binding proteins that regulate a plethora of essential cellular events, modulate the pathogenic process of AD. Among those, the small GTPase H-Ras, extensively studied in cancer, regulates synaptic function, and both upstream and downstream signaling pathways of H-Ras have been implicated in AD. However, the role of H-Ras *per se* in AD pathogenesis had not been explored previously. In the present study, the impact of *Hras* deletion on cognitive function and amyloid pathology was investigated in transgenic APP/PS1 mice of AD. Behavioral assessments showed that the absence of *Hras* rescued spatial memory deficit in APP/PS1 mice at 9 months of age. The pathological evaluation demonstrated that *Hras* deletion reduced cortical amyloid deposition and astrogliosis. Furthermore, *Hras* deficiency protected against amyloid plaque-associated loss of dendritic spines in APP/PS1 mice. Intriguingly, canonical signaling pathways downstream of H-Ras were not affected by the absence of *Hras* in the brain. Unbiased transcriptomic analysis revealed that lack of H-Ras affected the

Ling Li, lil@umn.edu.

Author Contribution WQ performed or participated in all experiments, analyzed the data, interpreted the results, and wrote the manuscript. AJ assisted ELISA, RNA extraction, and RNA-seq data analysis. RZ imaged and quantified plaque-associated/clustering microglia. JST conducted co-immunostaining of CD68 along with 6E10 and IBA1. AG maintained and genotyped experimental mice and collected tissue samples. LL conceived the study, supervised the progress of all experiments, and edited and finalized the manuscript. All authors reviewed the manuscript.

Supplementary Information The online version contains supplementary material available at https://doi.org/10.1007/s12035-022-03082-0.

Ethics Approval All animal procedures were reviewed and approved by the Institutional Animal Care and Use Committee (IACUC) at the University of Minnesota.

Consent for Publication All authors have reviewed and approved the manuscript.

Competing Interests The authors have no relevant financial or non-financial interests to disclose.

expression of select genes in the brain of AD mice and identified a novel connection between H-Ras and Annexin A4, a calcium-dependent phospholipid-binding protein that has been shown to regulate membrane repair, neuroinflammation, and calcium homeostasis. Taken together, these data indicate that H-Ras modifies the pathogenic process of AD and may serve as a potential therapeutic target for AD.

Keywords

Small GTPase; H-Ras; Cognitive function; Neuropathology; Transgenic mice; Alzheimer's disease

Introduction

Alzheimer's disease (AD) is the most common cause of dementia, affecting millions of people without a cure [1]. Neuropathological features in AD include amyloid plaques, neurofibrillary tangles, neuroinflammation, and synaptic dysfunction [2]. Although the molecular underpinning of AD is incompletely understood, mounting evidence suggests that Ras proteins and related pathways modify the pathogenic process of AD [3, 4].

Ras proteins are small GTPases that function as molecular switches to regulate cellular signal transduction [5]. They undergo post-translational lipid modifications, including protein prenylation (farnesylation by farnesyltransferase (FT) or geranylgeranylation by geranylgeranyl transferase-1 (GGT)), which are required for their proper cellular membrane localization and function. Ras has three isoforms (H-Ras, K-Ras, and N-Ras), all of which have received tremendous attention due to their frequent oncogenic mutations in human cancer and tumor cases [6]. K-Ras and N-Ras can be prenylated by GGT in the absence of FT, whereas H-Ras is exclusively prenylated by FT. Recently, we have shown that heterozygous deletion of FT, but not GGT, rescues memory deficits and reduces amyloid pathology in APP/PS1 mice and that farnesylated H-Ras is elevated in human AD brains [7, 8], indicating the potential involvement of H-Ras in the pathogenesis of AD.

H-Ras is dispensable during neurodevelopment and is highly expressed in the adult brains. H-Ras negatively regulates synaptic plasticity and memory formation under physiological conditions [9]. Gain-of-function mutations in H-Ras cause cancers and Costello syndrome, with features including mental retardation [10], and hyperactivity of Ras underlies neuronal dysfunction and cognitive impairment in neurofibromatosis type 1 [11, 12].

The ERK/MAPK and PI3K/AKT signaling cascades are two major canonical pathways downstream of H-Ras and both pathways significantly contribute to the pathogenesis of AD and other neurodegenerative diseases. The ERK/MAPK pathway is elevated in human AD brains and Aβ induced hyperactivation of Ras-ERK signaling can be alleviated by FT inhibition, hinting the involvement of farnesylated H-Ras [13, 14]. The Ras-ERK signaling cascade can crosstalk with another major pathway downstream of H-Ras, the PI3K/AKT pathway, which may contribute to AD pathogenesis by suppressing the induction of autophagy, an essential cellular clearance process that regulates Aβ secretion and clearance [15].

Since both farnesylation (upstream of H-Ras) and ERK/MAPK or PI3K/AKT signaling (downstream of H-Ras) have been implicated in AD, the absence of H-Ras *per se* is expected to ameliorate AD progression. To define the role of H-Ras in AD pathogenesis, APP/PS1 mice were crossed with *Hras*-null mice to generate different genotypes of mice, followed by assessments for cognitive function, pathology, and signal transduction. As expected, *Hras* deletion rescued memory retention deficits and reduced cortical amyloid deposition in AD mice. Further, dendritic spines near amyloid plaques were protected in *Hras*-null APP/PS1 mice. Surprisingly, *Hras* deletion had no significant effects on the ERK/MAPK and PI3K/AKT pathways. Transcriptomic analysis showed that lack of H-Ras modified the expression of select genes, including a significant elevation in the expression of *Anxa4*, which encodes Annexin A4 that regulates membrane repair, neuroinflammation, and calcium homeostasis. Taken together, these findings indicate that H-Ras modifies the pathogenic process of AD through non-canonical mechanisms, presenting H-Ras as a potential therapeutic target for tackling AD.

Methods

Animals

Hras-knockout (*Hras*−/−) (B6.129X1-*Hras1*^{tm1Esn}/Mmnc, stock # 030023-UNC) mice and the APP/PS1 (B6C3-Tg (APPswe, PSEN1dE9) 85Dbo/J; stock number 004462; now JAX MMRRC Stock # 034829) were described previously [16-18]. *Hras*-knockout AD mice were generated by the two-step breeding of APP/PS1 mice with *Hras+/−* mice. Six genotypes were produced including wild-type (WT) mice, *Hras+/−, Hras−/−,* APP/PS1, APP/PS1 *Hras+/−,* and APP/PS1 *Hras−/−*. Littermates were used whenever possible to minimize the potential confounding effects of genetic backgrounds. Both males and females are included in this study and a balanced gender design was applied whenever possible to all groups. Genomic DNA was isolated from ear biopsies and PCR analysis was used to determine the genotypes of the mice. Experiments in this study were conducted blind to genotypes and all animal procedures were reviewed and approved by the Institutional Animal Care and Use Committee (IACUC) at the University of Minnesota.

Behavioral Assessment

A battery of behavioral tests was conducted at 9 months of age to evaluate the locomotive function, anxiety levels, and spatial learning and memory as previously reported [19, 20]. In brief, the open-field test was conducted to evaluate the locomotive function of mice, in which mice were put into a square open box to explore freely for 5 min for three consecutive days. The elevated plus-maze test was employed to assess the anxiety levels, in which mice were placed in a plus-shape maze to explore freely for 5 min for two consecutive days. The spatial learning and memory of mice were evaluated in the Morris water maze test, in which mice were placed in a basin of water located in a visual cue-enriched room. Mice were trained to locate a hidden platform one centimeter below the water surface for four trials a day for five consecutive days. A probe trial was carried out on day six to assess their memory retention by removing the hidden platform, in which their crosses over the previous platform location were recorded within 1 min. A visible trial was conducted 2 h after the probe trial to assess the visual acuity of mice.

Golgi Staining and Spine Density Quantification

Golgi impregnation combined with Thioflavin-S (Th-S) fluorescent staining was conducted as previously described with a few modifications [19, 21, 22]. The GolgiStain kit (#PK401A, FD NeuroTechnologies) was used along with 0.05% Th-S (Sigma-Aldrich, T1892-25G). Mice were deeply anesthetized with ketamine and xylazine and perfused with PBS. Half of the anterior brain was infused with an equal mix of solution A and B provided by the GolgiStain kit for 1 week followed by infusion of solution C for another 3 days. Brains were then sectioned in solution C at 150 μm thickness using a vibratome (Leica), and the sections were dried overnight on glass slides. Sections were then washed with ddH_2O twice followed by a 10-min submerging in an equal mix of solution D and E. Sections were washed in ddH_2O twice, and then stained with 0.05% Th-S in 50% ethanol with gentle stirring in the dark for 20 min. Slides were then washed with ddH_2O and dehydrated as described by the GolgiStain manual and sealed in the mounting media (Permount, Fisher Scientific). Slides were dried for at least 3 days at 4°C then the edge of the coverslips was sealed with clear nail polish.

Golgi-stained sections were imaged under 100× bright field using the Keyence all-in-one fluorescent microscope (Keyence, BZ-X810). A z-stack of images that covers an entire dendritic branch on the z-plane with a step size of 1 μm was taken using the multi-stack module. Th-S staining was imaged using the GFP filter to determine the locations of amyloid plaques. All images of a dendritic branch were stacked in the Keyence Analysis software and exported for quantification in ImageJ. Secondary or above order of dendritic branches of the pyramidal neurons in the layer II/III of the anterior half of the cerebral cortex, including the somatosensory and primary motor areas, were imaged. The number of dendritic spines on a branch was manually counted, and the length of the branch was measured in ImageJ. “Distant” and “near” dendrites of plaques were determined in the close approximation of the border of an amyloid plaque. The dendritic branches 50 μm away from the border of any amyloid plaques were defined as “distant” and the dendritic branches within 50 μm of an amyloid plaque were defined as “near”. On average, a length of 42 ± 0.12 μm dendritic segments was quantified. At least two apical and two basal dendritic branches of a neuron, ten neurons from each animal, and four animals per genotype were included.

Immunostaining and Quantification

Immunofluorescent staining was conducted as previously described [7, 23]. Briefly, the posterior half of the brain was fixed in 4% PFA and then sectioned in PBS using a vibratome (Leica) at 50 μm thickness. Free-floating sections were treated for 7 min in 88% formic acid to enhance the detection of aggregated amyloid plaques. After being washed three times in PBS followed by 1-h blocking, sections were incubated in primary antibodies overnight. The primary antibodies included mouse 6E10 (Biolegend), rabbit anti-IBA1 (Wako), chicken anti-GFAP (Aves labs), rat anti-CD68 (Biolegend), and mouse anti-Lamp1 (University of Iowa Developmental Studies Hybridoma Bank). After the incubation with primary antibodies (sections incubated with primary antibodies omitted were included as controls), a mixture of anti-mouse Alexa Fluor 488, anti-rabbit or anti-rat Alexa Fluor 568, and anti-chicken Alexa Fluor 647 secondary antibodies (Invitrogen) were applied for 1 h at

room temperature. Sections were then washed three times in PBS and mounted onto glass slides. Sections were dried for half an hour and then sealed in the Vectashield HardSet antifade mounting medium with DAPI. X-34, a Congo red-derived dye, was also used to stain dense core amyloid plaques [24, 25].

The sections were imaged using the Keyence microscope. The entire section was scanned under a 10x objective lens and a stitched image was produced in the Keyence Analysis software. Stitched images were further processed and quantified in ImageJ. The background was subtracted using the rolling ball method and the same threshold was applied to all sections in ImageJ. The percentage of the stained area was then calculated in both the cortex and hippocampus. Four sections per animal were stained, analyzed, and averaged. Six animals per genotype were included.

To quantify plaque associated/clustering IBA1+ microglia, 6–8 images with visual fields of 720 μm × 540 μm were acquired for each mouse brain sections using the Keyence microscope (Keyence, BZ-X810) under a 20× objective lens in the cortical and hippocampal regions, respectively. ImageJ/FIJI was utilized for image processing and quantifications as previously described [26] with some modifications. Briefly, images were converted to 16-bit greyscale followed by background subtraction using the rolling ball method and contrast enhancement. A threshold determined by the built-in Moments algorithm was then applied to all images to create the segmentation mask, which is followed by a morphological opening. The immunostaining from the images was then segmented with Distance Transform Watershed. For 6E10+ plaques, a minimum size of 30 μm^2 was applied to exclude small areas of staining and the plaque masks were then enlarged by 10 μm. Plaque-associated IBA1+ microglia staining was confined and quantified within the enlarged area and normalized to the 6E10+ plaque area.

Total Protein and Synaptosome Isolation and Immunoblotting

Synaptosome and total protein isolation were conducted as previously described [19]. In brief, the anterior half of the cortex was homogenized on ice in a sucrose buffer. Samples were then incubated on ice for 10 min followed by 10 min centrifugation at 700 × g at 4°C. The pellet was homogenized and centrifuged again, and the supernatant was combined, from which total protein analysis proceeded. The rest of the supernatant was then centrifuged at 12,000 × g for 20 min at 4°C. The pellet contains enriched synaptosomes, which were then resuspended in the sucrose buffer supplemented with 1% triton x-100 and incubated on ice for 1 h.

The enriched synaptosome and total protein fractions were then subjected to protein assay and immunoblotting as previously described [7, 19]. Protein concentration was determined using Bradford assay (ThermoFisher) and then proteins were separated by 12% sodium dodecyl sulfate-polyacrylamide gel electrophoresis (SDS-PAGE) and transferred to PVDF membranes. The membranes were incubated in primary antibody overnight, washed, and incubated with corresponding HRP-conjugated secondary antibodies. The following primary antibodies were used: β-amyloid precursor protein (β-APP) (CT695, Invitrogen); total Ras (3965S, Cell Signaling); H-Ras (18295-1-AP, Proteintech); phospho-Akt (Ser473) (4060S, Cell Signaling); pan AKT (2920S, Cell Signaling); phospho-p44/42 MAPK

(Erk1/2) (Thr202/Tyr204) (4370S, Cell Signaling); p44/42 MAPK (ERK1/2) (9102S, Cell Signaling); phospho-S6 Ribosomal Protein (Ser235/236) (2211S, Cell Signaling); total S6 Ribosomal Protein (2217S, Cell Signaling); LC3 (L8918-25ULl Millipore); GAPDH (AM4300; Invitrogen); actin (MA5-15739; Invitrogen); GFAP (Aves Labs); IBA1 (016-20001, for Western Blotting, Wako); p53 (2524S, Cell Signaling); cyclin D1(55506S, Cell signaling); beclin 1 (NB500-249, Novus Biologicals); p62 (H00008878-M01, Novus Biologicals); PSD95 (MAB1598, Millipore Sigma); NR2A (07-632, Millipore Sigma); NR2B (MAB5778, Millipore Sigma); glutamate receptor 1 (GluA1) (AB1504, Millipore Sigma); synapsin I (AB1543, Millipore Sigma); and Annexin A4 (AF4146, R&D Systems). The membranes were treated with the Clarity Western ECL substrate (Bio-Rad). Signals were imaged using the iBright imaging system (ThermoFisher) and quantification of specific protein bands was achieved by densitometry analysis using the ImageJ software.

Aβ ELISA

The posterior part of the cortex was cut in half and the two pieces were processed for Aβ ELISA and RNA isolation, respectively. For the ELISA fraction, samples were further processed and separated into the carbonate-soluble and insoluble (guanidine (GnHCl)-soluble) fractions as previously described [27]. $A\beta_{40}$ and $A\beta_{42}$ were measured using ELISA kits (Invitrogen) according to the protocol provided by the manufacturer.

RNA Extraction, Sequencing, and Data Analysis

Total RNA was isolated from the other half of the posterior cortex using the RNA tissue isolation kit (732-6830; Bio-Rad). RNA quality, RNA-seq library preparation, and sequencing were conducted at the University of Minnesota Genomics Center as previously described [8]. Briefly, RNA quality was determined using the Quant-iT RiboGreen Assay Kit (ThermoFisher) and the Agilent Bioanalyzer system. Samples with an RNA integrity number (RIN) value of 7.8 or greater were included in this study. The Illumina TruSeq Stranded mRNA Kit and the Illumina NovaSeq 6000 platform were used to generate and sequence RNA sequencing libraries, respectively. Each sample generates 20 million reads on a 150-bp paired-end run.

Transcriptomic Analysis

Trimmomatic was used to trim reads and Hisat2 was used to align reads to the mouse genome using the GRCm38 reference, after which FeatureCounts was used to generate read counts by the Genomics Center as previously described [8]. Differential expression analysis was conducted using an integrated browser application iDEP (integrated Differential Expression and Pathway analysis) or using DESeq2 in R [28]. 0.5 minimal counts per million (CPM) in at least one library were set in pre-process data interface. A heatmap was generated to include the top 50 and bottom 50 variable genes based on the signal-to-noise ratio. Differentially expressed genes (DEGs) were identified with the iDEP build-in DESeq2 package using a threshold of false discovery rate (FDR) < 0.1 and setting genotype as the main factor, adjusting for sex. The raw RNA-seq datasets are available in the Gene Expression Omnibus repository (GEO Series accession number GSE180103).

Statistical Analysis

Data are expressed as means ± standard error. Statistical tests were carried out using R and GraphPad Prism 8. For comparing multiple groups, one-way ANOVA followed by Tukey's HSD post hoc test was used. For comparisons of behavioral performance over consecutive days, repeated measures two-way ANOVA was conducted. To compare the differences between the two groups, the Student's ***t***-test was used. The ***p***-value < 0.05 was considered statistically significant.

Results

Hras Deletion Rescues Spatial Memory Retention Deficits in APP/PS1 Mice

To evaluate the effect of *Hras* deletion on cognitive function in AD mice, a battery of behavioral tests was conducted with littermates of WT, *Hras*−/−, APP/PS1, and APP/PS1 *Hras*−/− mice at 9 months of age. The open-field test over three consecutive days was conducted to assess the general motor activity and the locomotive habituation response to environmental stimuli. No statistically significant differences were observed among different genotypes (Fig. 1a), suggesting that *Hras* deletion did not affect the locomotive response of mice. The elevated plus-maze was employed next for two consecutive days to evaluate the anxiety levels in mice. A comparable percentage of time mice spent in the open arm among different genotypes indicated that *Hras* deletion did not affect the anxiety levels of mice (Fig. 1b). Hippocampus-dependent learning and memory loss is a major cognitive deficit readout in AD and is recapitulated in the APP/PS1 mouse model [7]. Therefore, the Morris water maze test was conducted next to evaluate the hippocampal spatial learning and memory. No statistically significant differences were observed among different groups during the learning acquisition phase (Fig. 1c), indicating comparable learning capacities. During the probe trial, WT and *Hras*−/− showed comparable platform crossover, suggesting that H-Ras was not required for memory recall under physiological conditions. As expected, APP/PS1 mice showed memory retention deficits during the probe trial compared with WT, and importantly, APP/PS1 *Hras*−/− performed significantly better than APP/PS1 mice (Fig. 1d) and restored to the similar level of performance as WT mice. No differences in the average swimming speeds during the probe trial (WT: 0.177 ± 0.015 m/s; *Hras*−/−: 0.194 ± 0.01 m/s; APP/PS1: 0.224 ± 0.021 m/s; APP/PS1 *Hras*−/−: 0.186 ± 0.004 m/s) or the escape latencies during the visible platform trial among groups were observed (WT: 20.24 ± 3.38 s; *Hras*−/−: 19.4 ± 5.12 s; APP/PS1: 9.13 ± 1.56 s; APP/PS1 *Hras*−/−: 12.1 ± 1.57 s). The results indicate that the rescue of memory function in APP/PS1 *Hras*−/− mice was independent of any differences in non-cognitive parameters such as swimming ability or visual acuity of the mice.

Hras Deletion Reduces Cortical Amyloid Deposition and Astrogliosis

Amyloid deposition and excessive gliosis are key pathological features of AD and are associated with cognitive decline in AD [29]. To determine the cellular mechanisms underlying the cognitive beneficial effects in *Hras* deficient AD mice, neuropathology and neuroinflammation were evaluated. Robust amyloid deposition and microglial and astrocyte activation were confirmed in APP/PS1 mice compared with WT littermates (Online Resource, Fig. S1). Interestingly, amyloid deposition measured by 6E10 immunostaining

was significantly reduced in the cortex but not in the hippocampus of APP/PS1 *Hras−/−* compared with their APP/PS1 littermate controls (Fig. 2a, b). X-34 staining showed a trend decrease in the stained area in APP/PS1 *Hras−/−* mice compared with APP/PS1 (Online resource, Fig. S2), indicating that *Hras* deletion does not significantly influence the dense-core amyloid plaque load and the difference observed in the 6E10-stained area mostly likely resulted from the reduction of diffuse plaques. Microgliosis was assessed by IBA1 immunostaining and no difference was observed between APP/PS1 *Hras−/−* and APP/PS1 in either cortex or hippocampus (Fig. 2a, b). In contrast, astrogliosis, evaluated by GFAP immunostaining, was ameliorated in both cortex and hippocampus in APP/PS1 *Hras−/−* mice (Fig. 2a, b). Confocal microscopy demonstrated the reduction of both 6E10 positive amyloid plaques and plaque-associated astrogliosis in the cortex (Fig. 2c). Immunoblot analysis further confirmed the reduction of the reactive astrogliosis marker, GFAP, but not the microgliosis marker, IBA1, in the cortical lysate of APP/PS1 *Hras−/−* mice compared with APP/PS1 controls (Fig. 2d, e). To analyze microglia clustering around amyloid plaques in more detail, plaque-associated IBA1+ microglia were imaged and quantified. Consistently, the results showed no significant differences between APP/PS1 and APP/PS1 *Hras−/−* mice (Online Resource, Fig. S3). Furthermore, brain sections were also subjected to co-staining with activated microglial marker CD68 along with 6E10 and IBA1. The results showed that essentially all plaque-associated IBA+ microglia co-localized with CD68+ microglia (Online Resource, Fig. S4), confirming their activation status. Taken together, these data demonstrated that the absence of H-Ras led to the attenuation of cortical amyloid deposition and astrogliosis in APP/PS1 mice.

Hras Deletion Does Not Affect APP Expression and Processing or Overall Aβ Levels

Aβ is produced by the sequential cleavage of amyloid-β precursor protein (APP) by β-secretase that produces the β-C-terminal fragment (β-CTF) first and then by γ-secretase [30]. APP can also be processed through the non-amyloidogenic pathway by the sequential cleavage by α-secretase first that produces α-CTF, followed by γ-secretase. To evaluate the impact of *Hras* deletion on the expression of full-length APP and its proteolytic processing, immunoblot analysis was performed with brain tissue lysates. The results showed no statistically significant differences in the overall expression of APP (Fig. 3a, b) or its amyloidogenic and non-amyloidogenic cleavage measured by the ratio of β-CTF/α-CTF (Fig. 3a, b) between APP/PS1 *Hras−/−* and APP/PS1 mice.

Among Aβ isoforms, $A\beta_{40}$ and $A\beta_{42}$ have been intensely studied due to their close relationship with the progression and neuropathology of AD [31]. Familial AD mutations often lead to elevated $A\beta_{42}/A\beta_{40}$ ratio and soluble $A\beta_{42}$ is believed to be more neurotoxic compared with aggregated fibrillary forms of Aβ [31]. Therefore, soluble (carbonate-soluble) and insoluble (guanidine (GnHCl)-soluble) $A\beta_{40}$ and $A\beta_{42}$ levels were evaluated using ELISA. Interestingly, although cortical amyloid deposition was reduced as shown by immunostaining, neither carbonate-soluble nor insoluble fractions of $A\beta_{40}$ or $A\beta_{42}$ levels, the total $A\beta_{40}$ and $A\beta_{42}$ levels, or the $A\beta_{42}/A\beta_{40}$ ratios were altered in the cortical lysate of APP/PS1 *Hras−/−* mice compared with APP/PS1 mice (Fig. 3c). These results suggest that *Hras* deficiency had limited impact on the overall Aβ levels in the brain.

Hras Deletion Protects Against Dendritic Spine Loss Near Amyloid Plaques Without Changing Overall Spine Density or Synaptic Protein Expression

Glutamatergic neurotransmission dictates synaptic function and cognitive performance. To evaluate the outcome of *Hras* deficiency on synaptic makers, immunoblotting was conducted on synaptosomes isolated from cortical lysates. Compared with APP/PS1 mice, APP/PS1 *Hras*−/− mice showed similar expression of synaptic markers, including excitatory scaffolding protein PSD95, presynaptic marker synapsin 1 (Syn1), AMPA receptor subunit GluA1, or NMDA subunit NR2A and NR2B (Fig. 4a, b). These data suggest that *Hras* deficiency had no effect on the expression of these synaptic proteins.

Loss of synapses is a hallmark of AD and dendritic spines are strongly influenced by nearby amyloid plaques [22]. To evaluate the influence of *Hras* deficiency on dendritic spine density in the brain of APP/PS1 mice, Golgi-Cox impregnation combined with Th-S co-staining was employed to visualize dendritic spines and fibrillar amyloid plaques (Fig. 4c; Online resource, Fig. S5). As expected, the overall spine density is significantly decreased in APP/PS1 mice compared with WT in both cortical apical and basal pyramidal neurons in the layer II/III of the frontal cortex (Fig. 4d-f). *Hras* deficiency did not significantly affect overall spine density when compared between WT and *Hras*−/− or between APP/PS1 mice and APP/PS1 *Hras*−/− mice (Fig. 4d-f). However, when the spine density was quantified respectively in dendritic branches near (≤ 50 μm) versus distant (> 50 μm) from amyloid plaques indicated by Th-S staining as previously described [21, 22], the results showed that the spine density was significantly higher in both apical and basal dendrites near amyloid plaques in APP/PS1 *Hras*−/− than in APP/PS1, whereas the spine density in either apical or basal dendrites distant from amyloid plaques remained similar in APP/PS1 and APP/PS1 *Hras*−/− (Fig. 4d-f). These results indicate that *Hras* deficiency protects dendritic spines from Aβ toxicity and reduces spine loss near amyloid plaques.

In addition, to examine whether *Hras* deletion affects dendritic dystrophy, brain sections were subjected to immunostaining for Lamp1, a marker for late endosome that has been widely used to assess neurite dystrophy [26, 32]. The results showed no difference in the Lamp1-stained area in APP/PS1 *Hras*−/− compared with APP/PS1 mice (Online Resource, Fig. S2), indicating that loss of H-Ras does not affect the overall neurite dystrophy but preserves synaptic spines on dendrites in the vicinity of amyloid plaques in APP/PS1mice.

Hras Deletion Does Not Affect the MAPK/ERK or the PI3K/AKT Pathway

H-Ras is a well-known regulator of the ERK/MAPK and the PI3K/AKT pathway and both pathways have been implicated in the pathogenesis of AD [6, 33]. The levels of total and phosphorylated ERK (p-ERK) and key cell-cycle regulators (Fig. 5a), including cyclin D1, total and phosphorylated retinoblastoma protein (Rb), and p53, were evaluated by immunoblot analysis of cortical lysates. Surprisingly, the p-ERK levels were comparable between APP/PS1 *Hras*−/− mice and APP/PS1 mice (Fig. 5b, c), suggesting that *Hras* deficiency does not alter the ERK/MAPK signaling in the brain of AD mice. Consistently, none of the protein levels of cell cycle regulators was different between APP/PS1 *Hras*−/− mice and APP/PS1 mice (Fig. 5b, c).

H-Ras has also been identified as a key activator of the PI3K/AKT pathway, which can lead to the activation of the mTOR signaling and regulation of autophagy [6] (Fig. 5d). Therefore, protein levels of key molecules in the PI3K/ AKT-mTOR pathway and autophagy were evaluated next. Interestingly, the p-AKT level showed a trend of increase in the APP/PS1 *Hras−/−* mice compared with APP/PS1 controls (Fig. 5e, f). However, the slightly elevated p-AKT levels in APP/PS1 *Hras−/−* mice did not alter the downstream signaling of mTOR, including the p-S6 levels, or the autophagy regulators, including p62, Beclin1, and LC3 (Fig. 5e, f). These data indicate that *Hras* deficiency is not sufficient to alter the ERK/MAPK and PI3K/AKT signaling in AD brains and compensatory mechanisms exist to offset the loss of H-Ras. In addition to H-Ras, the Ras proteins consist of two other isoforms, K-Ras and N-Ras, which may be upregulated in the absence of H-Ras (Fig. 5g). To test this idea, H-Ras, and total Ras levels were assessed by immunoblotting. As expected, the H-Ras protein was absent in the APP/PS1 *Hras−/−* mice. Without H-Ras, the total Ras level in the brain decreased by ~ 50% (Fig. 5h, i), suggesting that K-Ras and N-Ras were not overexpressed to compensate the loss of H-Ras. Alternatively, the remaining pan-Ras level was sufficient to drive the activation of ERK/MAPK and the PI3K/AKT pathways. In addition, the APP/PS1 transgenes and/or amyloid pathology did not affect the overall protein expression of H-Ras or pan-Ras in these mice (Online Resource, Fig. S6).

Ablation of *Hras* Modifies the Expression of Select Genes in the Brain of APP/PS1 Mice

To further elucidate potential molecular mechanisms and signaling cascades in *Hras* deficient AD mice, unbiased transcriptomic profiling was performed with the cortical tissue of APP/PS1 and APP/PS1 *Hras−/−* mice. Interestingly, although *Hras* deficiency altered some gene expression as shown on the heatmap with the top 100 most variable genes (Fig. 6a), differentially expressed genes (DEGs) analysis only identified 10 significantly altered (FDR < 0.1) in the APP/PS1 *Hras−/−* mice compared with APP/PS1, suggesting that lack of H-Ras had a limited impact on the overall transcriptomic landscape. Out of the 10 DEGs, four were downregulated, including *Hras*, and six were upregulated (Table 1). Notably, a housekeeping gene, *Gapdh*, was significantly down-regulated in APP/PS1 *Hras−/−* mice. However, protein levels of GAPDH were comparable between genotypes by immunoblotting analysis when normalized to actin or tubulin, whose transcription was not altered in *Hras−/−* AD mice (Fig. 6b, c). This result suggests that post-transcriptional mechanisms might be involved in maintaining the protein level of GAPDH. Intriguingly, the expression of *Anxa4* (encoding Annexin A4) was significantly upregulated in *Hras*-null AD mouse brains (Table 1). Annexin A4 plays a prominent role in several biological functions, including membrane repair, Ca^{2+} homeostasis, and regulation of neuroinflammatory pathways [34-36]. Immunoblotting confirms the upregulation of Annexin A4 at the protein level (Fig. 6b,c). The increase in the expression of Annexin A4 might have conferred beneficial outcomes in the brain of APP/PS1 *Hras−/−* mice. However, further studies are required to elucidate the significance of the novel connections identified between *Anxa4*, or other DEGs, and H-Ras or its downstream signaling pathways.

Discussion

Findings from this study support the role of the small GTPase H-Ras, an exclusively farnesylated protein, in the pathogenesis of AD. Studies from our laboratory have consistently shown that inhibition of the farnesylation pathway leads to beneficial cognitive outcomes and ameliorated AD pathology [7, 8]. Others have reported that elevated Ras expression is an early event in human AD brains and is associated with amyloid plaque depositions [43]. Farnesylated H-Ras level is elevated in human AD brains and the well-known H-Ras downstream signaling cascades, ERK/MAPK, and PI3K-AKT pathways are implicated in AD pathogenesis. However, the direct role of H-Ras in AD pathogenesis had not been explored *in vivo* prior to this study. The results revealed that *Hras* deletion rescued memory consolidation deficits and reduced cortical amyloid deposition in AD mice. Further, dendritic spines near amyloid plaques were protected in *Hras*-null APP/PS1 mice without overall changes in dendritic dystrophy. Notably, *Hras* deletion had no significant effects on the ERK/MAPK and PI3K/AKT pathways. Lack of H-Ras affected the expression of select genes in AD mice, including a significant elevation in the expression of *Anxa4*, which plays an important role in mediating membrane repair, neuroinflammation, and calcium homeostasis. The beneficial outcomes of *Hras* deletion in AD mice partially overlap with previous findings from our laboratory that FT reduction ameliorates the pathogenic process of AD, suggesting that controlling H-Ras farnesylation/function constitutes one of the potential mechanisms underlying the beneficial effects of FT inhibition in AD.

The finding that amyloid deposition was reduced in the cortex of *Hras* deficient AD mice but not in the hippocampus assessed by 6E10 immunostaining indicates brain regional differences in response to *Hras* deficiency. Interestingly, the total Aβ levels were not altered in the cortex of *Hras* deficient AD mice measured by ELISA. The discrepancy between amyloid deposition assessed by immunostaining on brain sections and Aβ levels assessed by ELISA of total cortical homogenates might be caused by potentially modified distributions of intercellular Aβ and extracellular plaque deposition in APP/PS1 *Hras*$^{-/-}$ mice. Of note, astrogliosis but not plaque-associated microgliosis was strongly influenced by *Hras* deficiency. While microglia play important roles in mediating amyloid phagocytosis, astrogliosis is an early event in the AD brains that can also contribute to amyloid phagocytosis [44]. Despite the ability to engulf Aβ, astrocytes store rather than degrade Aβ, which results in secreting microvesicles comprising of truncated Aβ, which can induce neuronal apoptosis and exacerbate AD pathology [45]. Thus, reduced astrogliosis in APP/PS1 *Hras*$^{-/-}$ mice is likely beneficial. The cell-type-specific roles of H-Ras in AD pathogenesis remain to be explored.

Interestingly, neither p-ERK nor p-AKT levels nor the expression of their downstream signaling proteins were altered in *Hras* deficient AD brain. H-Ras is a well-known oncogenic gene due to its frequent mutagenesis in human cancers and its importance in regulating the cell cycle [6]. Dissociation of H-Ras from plasma membrane raft in baby hamster kidney (BHK) cells diminished the p-ERK levels [46]. Depleting H-Ras in head and neck squamous cell carcinoma (HNSCC) abolished the PI3K-AKT signaling [47]. Several reports have shown that increased H-Ras signaling is associated with elevated ERK and AKT signaling both *in vivo* and *in vitro* [6, 48, 49]. However, p-ERK and p-AKT levels

were similar to WT mice in the brain, heart, and kidney of 2-month-old *Hras*−/− mice or in mice expressing constitutively active mutant H-Ras [50]. Consistently, the effectors of the MAPK/ERK and PI3K-AKT signaling cascades did not change in the brain of APP/PS1 *Hras*−/− mice in this study. These results suggest that compensatory mechanisms exist to offset the loss of H-Ras. In addition to H-Ras, the Ras family of proteins consists of two other isoforms, K-Ras and N-Ras. Unlike H-Ras, K-Ras and H-Ras can be prenylated by GGT in the absence of FT. H-Ras and N-Ras are dispensable during neurodevelopment while K-Ras alone is necessary and sufficient to drive normal development in mice [16]. In the brain of APP/PS1 mice, *Hras* knockout accounted for approximately half of the decrease in total Ras protein level and transcriptomic analysis showed no changes in the gene expression of K-Ras or N-Ras. These results indicate that K-Ras or N-Ras was not overexpressed to compensate for the loss of H-Ras. It is possible that the reduced total level of Ras was sufficient to drive the activation of ERK and AKT signaling. The precise molecular mechanisms that drive the MAPK/ERK and PI3K-AKT pathways in the absence of H-Ras remain to be further explored.

H-Ras has been shown to play an important role in modulating synaptic and cognitive function but results are not consistent across different studies. *Hras*-null mice showed upregulated NMDA receptor-mediated synaptic response and enhanced hippocampal long-term potentiation (LTP) using high-frequency stimulation (HFS) [51]. However, low-frequency stimulation (LFS) in a combination of postsynaptic depolarization-induced LTP was comparable between *Hras*-null mice and WT [52], indicating stimulation protocol-dependent effects of *Hras* deficiency. Constitutively active transgenic *Hras* mice ($Hras^{G12V}$) have been shown to regulate synapsin I activity in the presynapses that leads to enhanced hippocampal-dependent learning and memory [53]. In contrast, targeted replacement of constitutively active *Hras* mice ($Hras^{G12v/G12v}$) showed brain atrophy and impaired learning and memory in the Morris water maze test [54]. Of note, the aforementioned studies were all conducted under non-pathological conditions, and the present report is the first, to the best of our knowledge, to show the role of H-Ras in the context of AD pathology. *Hras* deletion rescued memory deficits in AD mice and conferred protection against dendritic spine loss near amyloid plaques, suggesting the beneficial neuronal and cognitive outcome of suppressing H-Ras. It is noteworthy that the APP/PS1 mouse model is primarily an amyloid model of AD. Given the broad involvement of H-Ras signaling pathways in cellular structure and function, the impact of *Hras* deletion on tau/tangle pathology warrants further investigation.

Unbiased transcriptomic analysis showed that the absence of H-Ras affected the expression of select genes in the brain of APP/PS1 mice. It identified a novel connection between *Hras* deficiency and the upregulation of *Anxa4*, which encodes for Annexin A4. Annexin A4 is mainly expressed in microglia and endothelial cells in the brain [55]. The function of Annexin A4 is less understood but it has emerged as an important player in plasma membrane repair [34]. Upon detecting Ca^{2+} influx, Annexin A4 is recruited to the cell surface to facilitate the membrane repair near Ca^{2+} influx. Annexin A4 has also been connected with the NF-κB pathway, which is important in regulating neuroinflammation that contributes to AD pathogenesis [35, 56]. The molecular mechanisms that connect H-Ras with Annexin A4 and the role of their interactions in AD remain to be elucidated.

In summary, the present study revealed the beneficial cognitive outcome of *Hras* deletion in a mouse model of AD. *Hras* deletion reduced the cortical amyloid deposition, alleviated astrogliosis, and protected against dendritic spine loss near amyloid plaques. *Hras* deletion provoked functional changes in neurons and glia and modified the expression of select genes in the brain of AD mice. One of the significantly altered genes was *Anxa4*, coding for Annexin A4 that is involved in the regulation of membrane repair, calcium homeostasis, and neuroinflammation. These findings provide novel insights into the role of H-Ras in the pathogenesis of AD and identify H-Ras as a potential therapeutic target for AD besides cancer.

Supplementary Material

Refer to Web version on PubMed Central for supplementary material.

Acknowledgements

We thank the University of Minnesota Informatics Institute and Juan E. Abrahante Llorens for the initial RNA-seq data analysis.

Funding

This work was supported in part by grants from the National Institute on Aging of the National Institutes of Health (RF1AG056976 and RF1AG058081), and the College of Pharmacy and the Office of Clinical Affairs Faculty Research Development Program at the University of Minnesota.

Data Availability

The datasets generated during and/or analyzed during the current study are available in the Gene Expression Omnibus repository (GEO Series accession number GSE180103).

References

1. Alzheimer's Association (2021) 2021 Alzheimer's disease facts and figures. Alzheimers Dement 17(3):327–406. 10.1002/alz.12328 [PubMed: 33756057]
2. Serrano-Pozo A, Frosch MP, Masliah E, Hyman BT (2011) Neuropathological alterations in Alzheimer disease. Cold Spring Harb Perspect Med 1(1):a006189. 10.1101/cshperspect.a006189 [PubMed: 22229116]
3. Hottman DA, Li L (2014) Protein prenylation and synaptic plasticity: implications for Alzheimer's disease. Mol Neurobiol 50(1):177–185. 10.1007/s12035-013-8627-z [PubMed: 24390573]
4. Weber AJ, Herskowitz JH (2021) Perspectives on ROCK2 as a Therapeutic Target for Alzheimer's Disease. Front Cell Neurosci 15:64
5. Schmidt A, Hall A (2002) Guanine nucleotide exchange factors for Rho GTPases: turning on the switch. Genes Dev 16(13):1587–1609. 10.1101/gad.1003302 [PubMed: 12101119]
6. Shu L, Wang D, Saba NF, Chen ZG (2020) A Historic Perspective and Overview of H-Ras Structure, Oncogenicity, and Targeting. Mol Cancer Ther 19(4):999–1007. 10.1158/1535-7163.MCT-19-0660 [PubMed: 32241873]
7. Cheng S, Cao D, Hottman DA, Yuan L, Bergo MO, Li L (2013) Farnesyltransferase haplodeficiency reduces neuropathology and rescues cognitive function in a mouse model of Alzheimer disease. J Biol Chem 288(50):35952–35960. 10.1074/jbc.M113.503904 [PubMed: 24136196]
8. Jeong A, Cheng S, Zhong R, Bennett DA, Bergö MO, Li L (2021) Protein farnesylation is upregulated in Alzheimer's human brains and neuron-specific suppression of farnesyltransferase

mitigates pathogenic processes in Alzheimer's model mice. Acta Neuropathol Commun 9(1):129. 10.1186/s40478-021-01231-5 [PubMed: 34315531]

9. Ye X, Carew TJ (2010) Small G protein signaling in neuronal plasticity and memory formation: the specific role of ras family proteins. Neuron 68(3):340–361 [PubMed: 21040840]
10. Gripp KW, Lin AE (2012) Costello syndrome: a Ras/mitogen activated protein kinase pathway syndrome (rasopathy) resulting from HRAS germline mutations. Genet Med: Off J Am Coll Med Genet 14(3):285–292. 10.1038/gim.0b013e31822dd91f
11. Costa RM, Federov NB, Kogan JH, Murphy GG, Stern J, Ohno M, Kucherlapati R, Jacks T et al. (2002) Mechanism for the learning deficits in a mouse model of neurofibromatosis type 1. Nature 415(6871):526–530 [PubMed: 11793011]
12. Li W, Cui Y, Kushner SA, Brown RA, Jentsch JD, Frankland PW, Cannon TD, Silva AJ (2005) The HMG-CoA reductase inhibitor lovastatin reverses the learning and attention deficits in a mouse model of neurofibromatosis type 1. Curr Biol 15(21):1961–1967 [PubMed: 16271875]
13. Perry G, Roder H, Nunomura A, Takeda A, Friedlich AL, Zhu X, Raina AK, Holbrook N et al. (1999) Activation of neuronal extracellular receptor kinase (ERK) in Alzheimer disease links oxidative stress to abnormal phosphorylation. NeuroReport 10(11):2411–2415 [PubMed: 10439473]
14. Chen MJ, Ramesha S, Weinstock LD, Gao T, Ping L, Xiao H, Dammer EB, Duong DD et al. (2019) Microglial ERK signaling is a critical regulator of pro-inflammatory immune responses in Alzheimer's disease. bioRxiv:798215
15. Nilsson P, Saido TC (2014) Dual roles for autophagy: degradation and secretion of Alzheimer's disease Abeta peptide. BioEssays 36(6):570–578. 10.1002/bies.201400002 [PubMed: 24711225]
16. Esteban LM, Vicario-Abejón C, Fernández-Salguero P, Fernández-Medarde A, Swaminathan N, Yienger K, Lopez E, Malumbres M et al. (2001) Targeted genomic disruption of H-ras and N-ras, individually or in combination, reveals the dispensability of both loci for mouse growth and development. Mol Cell Biol 21(5):1444–1452 [PubMed: 11238881]
17. Jankowsky JL, Slunt HH, Ratovitski T, Jenkins NA, Copeland NG, Borchelt DR (2001) Co-expression of multiple transgenes in mouse CNS: a comparison of strategies. Biomol Eng 17(6):157–165 [PubMed: 11337275]
18. Jankowsky JL, Fadale DJ, Anderson J, Xu GM, Gonzales V, Jenkins NA, Copeland NG, Lee MK et al. (2004) Mutant presenilins specifically elevate the levels of the 42 residue beta-amyloid peptide in vivo: evidence for augmentation of a 42-specific gamma secretase. Hum Mol Genet 13(2):159–170 [PubMed: 14645205]
19. Qu W, Li L (2020) Loss of TREM2 Confers Resilience to Synaptic and Cognitive Impairment in Aged Mice. J Neurosci 40(50):9552–9563. 10.1523/JNEUROSCI.2193-20.2020 [PubMed: 33139402]
20. Qu W, Suazo KF, Liu W, Cheng S, Jeong A, Hottman D, Yuan LL, Distefano MD et al. (2021) Neuronal Protein Farnesylation Regulates Hippocampal Synaptic Plasticity and Cognitive Function. Mol Neurobiol 58(3):1128–1144. 10.1007/s12035-020-02169-w [PubMed: 33098528]
21. Vints K, Vandael D, Baatsen P, Pavie B, Vernaillen F, Corthout N, Rybakin V, Munck S et al. (2019) Modernization of Golgi staining techniques for high-resolution, 3-dimensional imaging of individual neurons. Sci Rep 9(1):130. 10.1038/s41598-018-37377-x [PubMed: 30644431]
22. Kartalou GI, Endres T, Lessmann V, Gottmann K (2020) Golgi-Cox impregnation combined with fluorescence staining of amyloid plaques reveals local spine loss in an Alzheimer mouse model. J Neurosci Methods 341:108797. 10.1016/j.jneumeth.2020.108797 [PubMed: 32479974]
23. Qu W, Johnson A, Kim JH, Lukowicz A, Svedberg D, Cvetanovic M (2017) Inhibition of colony-stimulating factor 1 receptor early in disease ameliorates motor deficits in SCA1 mice. J Neuroinflammation 14(1):107. 10.1186/s12974-017-0880-z [PubMed: 28545543]
24. Styren SD, Hamilton RL, Styren GC, Klunk WE (2000) X-34, a fluorescent derivative of Congo red: a novel histochemical stain for Alzheimer's disease pathology. J Histochem Cytochem 48(9):1223–1232 [PubMed: 10950879]
25. Ulrich JD, Ulland TK, Mahan TE, Nyström S, Nilsson KP, Song WM, Zhou Y, Reinartz M et al. (2018) ApoE facilitates the microglial response to amyloid plaque pathology. J Exp Med 215(4):1047–1058 [PubMed: 29483128]

26. Meilandt WJ, Ngu H, Gogineni A, Lalehzadeh G, Lee S-H, Srinivasan K, Imperio J, Wu T et al. (2020) Trem2 deletion reduces late-stage amyloid plaque accumulation, elevates the Aβ42: Aβ40 ratio, and exacerbates axonal dystrophy and dendritic spine loss in the PS2APP Alzheimer's mouse model. J Neurosci 40(9):1956–1974 [PubMed: 31980586]
27. Cao D, Lu H, Lewis TL, Li L (2007) Intake of sucrose-sweetened water induces insulin resistance and exacerbates memory deficits and amyloidosis in a transgenic mouse model of Alzheimer disease. J Biol Chem 282(50):36275–36282 [PubMed: 17942401]
28. Ge SX, Son EW, Yao R (2018) iDEP: an integrated web application for differential expression and pathway analysis of RNA-Seq data. BMC Bioinformatics 19(1):534. 10.1186/s12859-018-2486-6 [PubMed: 30567491]
29. Carter SF, Herholz K, Rosa-Neto P, Pellerin L, Nordberg A, Zimmer ER (2019) Astrocyte Biomarkers in Alzheimer's Disease. Trends Mol Med 25(2):77–95. 10.1016/j.molmed.2018.11.006 [PubMed: 30611668]
30. O'Brien RJ, Wong PC (2011) Amyloid precursor protein processing and Alzheimer's disease. Annu Rev Neurosci 34:185–204. 10.1146/annurev-neuro-061010-113613 [PubMed: 21456963]
31. Selkoe DJ, Hardy J (2016) The amyloid hypothesis of Alzheimer's disease at 25 years. EMBO Mol Med 8(6):595–608 [PubMed: 27025652]
32. Gowrishankar S, Yuan P, Wu Y, Schrag M, Paradise S, Grutzendler J, De Camilli P, Ferguson SM (2015) Massive accumulation of luminal protease-deficient axonal lysosomes at Alzheimer's disease amyloid plaques. Proc Natl Acad Sci 112(28):E3699–E3708 [PubMed: 26124111]
33. Rai SN, Dilnashin H, Birla H, Singh SS, Zahra W, Rathore AS, Singh BK, Singh SP (2019) The Role of PI3K/Akt and ERK in Neurodegenerative Disorders. Neurotox Res 35(3):775–795. 10.1007/s12640-019-0003-y [PubMed: 30707354]
34. Boye TL, Maeda K, Pezeshkian W, Sonder SL, Haeger SC, Gerke V, Simonsen AC, Nylandsted J (2017) Annexin A4 and A6 induce membrane curvature and constriction during cell membrane repair. Nat Commun 8(1):1623. 10.1038/s41467-017-01743-6 [PubMed: 29158488]
35. Jeon Y-J, Kim D-H, Jung H, Chung SJ, Chi S-W, Cho S, Lee SC, Park BC et al. (2010) Annexin A4 interacts with the NF-κB p50 subunit and modulates NF-κB transcriptional activity in a Ca 2+-dependent manner. Cell Mol Life Sci 67(13):2271–2281 [PubMed: 20237821]
36. O'Leary NA, Wright MW, Brister JR, Ciufo S, Haddad D, McVeigh R, Rajput B, Robbertse B et al. (2016) Reference sequence (RefSeq) database at NCBI: current status, taxonomic expansion, and functional annotation. Nucleic Acids Res 44(D1):D733–D745 [PubMed: 26553804]
37. Poprzeczko M, Bicka M, Farahat H, Bazan R, Osinka A, Fabczak H, Joachimiak E, Wloga D (2019) Rare human diseases: model organisms in deciphering the molecular basis of primary ciliary dyskinesia. Cells 8(12):1614 [PubMed: 31835861]
38. Kim GW, Lin JE, Waldman SA (2013) GUCY2C: at the intersection of obesity and cancer. Trends Endocrinol Metab 24(4):165–173 [PubMed: 23375388]
39. Nicholls C, Li H, Liu JP (2012) GAPDH: a common enzyme with uncommon functions. Clin Exp Pharmacol Physiol 39(8):674–679. 10.1111/j.1440-1681.2011.05599.x [PubMed: 21895736]
40. Tristan C, Shahani N, Sedlak TW, Sawa A (2011) The diverse functions of GAPDH: views from different subcellular compartments. Cell Signal 23(2):317–323. 10.1016/j.cellsig.2010.08.003 [PubMed: 20727968]
41. Bellacosa A (2001) Role of MED1 (MBD4) Gene in DNA repair and human cancer. J Cell Physiol 187(2):137–144. 10.1002/jcp.1064 [PubMed: 11267993]
42. Box JM, Kaur J, Stuart RA (2017) MrpL35, a mitospecific component of mitoribosomes, plays a key role in cytochrome c oxidase assembly. Mol Biol Cell 28(24):3489–3499. 10.1091/mbc.E17-04-0239 [PubMed: 28931599]
43. Gartner U, Holzer M, Heumann R, Arendt T (1995) Induction of p21ras in Alzheimer pathology. NeuroReport 6(10):1441–1444 [PubMed: 7488744]
44. Gonzalez-Reyes RE, Nava-Mesa MO, Vargas-Sanchez K, Ariza-Salamanca D, Mora-Munoz L (2017) Involvement of Astrocytes in Alzheimer's Disease from a Neuroinflammatory and Oxidative Stress Perspective. Front Mol Neurosci 10:427. 10.3389/fnmol.2017.00427 [PubMed: 29311817]

45. Sollvander S, Nikitidou E, Brolin R, Soderberg L, Sehlin D, Lannfelt L, Erlandsson A (2016) Accumulation of amyloid-beta by astrocytes result in enlarged endosomes and microvesicle-induced apoptosis of neurons. Mol Neurodegener 11(1):38. 10.1186/s13024-016-0098-z [PubMed: 27176225]

46. Prior IA, Harding A, Yan J, Sluimer J, Parton RG, Hancock JF (2001) GTP-dependent segregation of H-ras from lipid rafts is required for biological activity. Nat Cell Biol 3(4):368–375 [PubMed: 11283610]

47. Geyer FC, Li A, Papanastasiou AD, Smith A, Selenica P, Burke KA, Edelweiss M, Wen H-C et al. (2018) Recurrent hotspot mutations in HRAS Q61 and PI3K-AKT pathway genes as drivers of breast adenomyoepitheliomas. Nat Commun 9(1):1–16 [PubMed: 29317637]

48. Chen X, Mitsutake N, LaPerle K, Akeno N, Zanzonico P, Longo VA, Mitsutake S, Kimura ET et al. (2009) Endogenous expression of HrasG12V induces developmental defects and neoplasms with copy number imbalances of the oncogene. Proc Natl Acad Sci 106(19):7979–7984 [PubMed: 19416908]

49. Suire S, Hawkins P, Stephens L (2002) Activation of phosphoinositide 3-kinase gamma by Ras. Curr Biol 12(13):1068–1075. 10.1016/s0960-9822(02)00933-8 [PubMed: 12121613]

50. Schuhmacher AJ, Guerra C, Sauzeau V, Canamero M, Bustelo XR, Barbacid M (2008) A mouse model for Costello syndrome reveals an Ang II-mediated hypertensive condition. J Clin Invest 118(6):2169–2179. 10.1172/JCI34385 [PubMed: 18483625]

51. Manabe T, Aiba A, Yamada A, Ichise T, Sakagami H, Kondo H, Katsuki M (2000) Regulation of long-term potentiation by H-Ras through NMDA receptor phosphorylation. J Neurosci 20(7):2504–2511 [PubMed: 10729330]

52. Komiyama NH, Watabe AM, Carlisle HJ, Porter K, Charlesworth P, Monti J, Strathdee DJ, O'Carroll CM et al. (2002) SynGAP regulates ERK/MAPK signaling, synaptic plasticity, and learning in the complex with postsynaptic density 95 and NMDA receptor. J Neurosci: Off J Soc Neurosci 22(22):9721–9732

53. Kushner SA, Elgersma Y, Murphy GG, Jaarsma D, van Woerden GM, Hojjati MR, Cui Y, LeBoutillier JC et al. (2005) Modulation of presynaptic plasticity and learning by the H-ras/extracellular signal-regulated kinase/synapsin I signaling pathway. J Neurosci: Off J Soc Neurosci 25(42):9721–9734. 10.1523/JNEUROSCI.2836-05.2005

54. Schreiber J, Grimbergen LA, Overwater I, Vaart TV, Stedehouder J, Schuhmacher AJ, Guerra C, Kushner SA et al. (2017) Mechanisms underlying cognitive deficits in a mouse model for Costello Syndrome are distinct from other RASopathy mouse models. Sci Rep 7(1):1256. 10.1038/s41598-017-01218-0 [PubMed: 28455524]

55. Zhang Y, Chen K, Sloan SA, Bennett ML, Scholze AR, O'Keeffe S, Phatnani HP, Guarnieri P et al. (2014) An RNA-sequencing transcriptome and splicing database of glia, neurons, and vascular cells of the cerebral cortex. J Neurosci: Off J Soc Neurosci 34(36):11929–11947. 10.1523/JNEUROSCI.1860-14.2014

56. Gold M, El Khoury J β-amyloid, microglia, and the inflammasome in Alzheimer's disease. In: Seminars in immunopathology, 2015. vol 6. Springer, pp 607–611

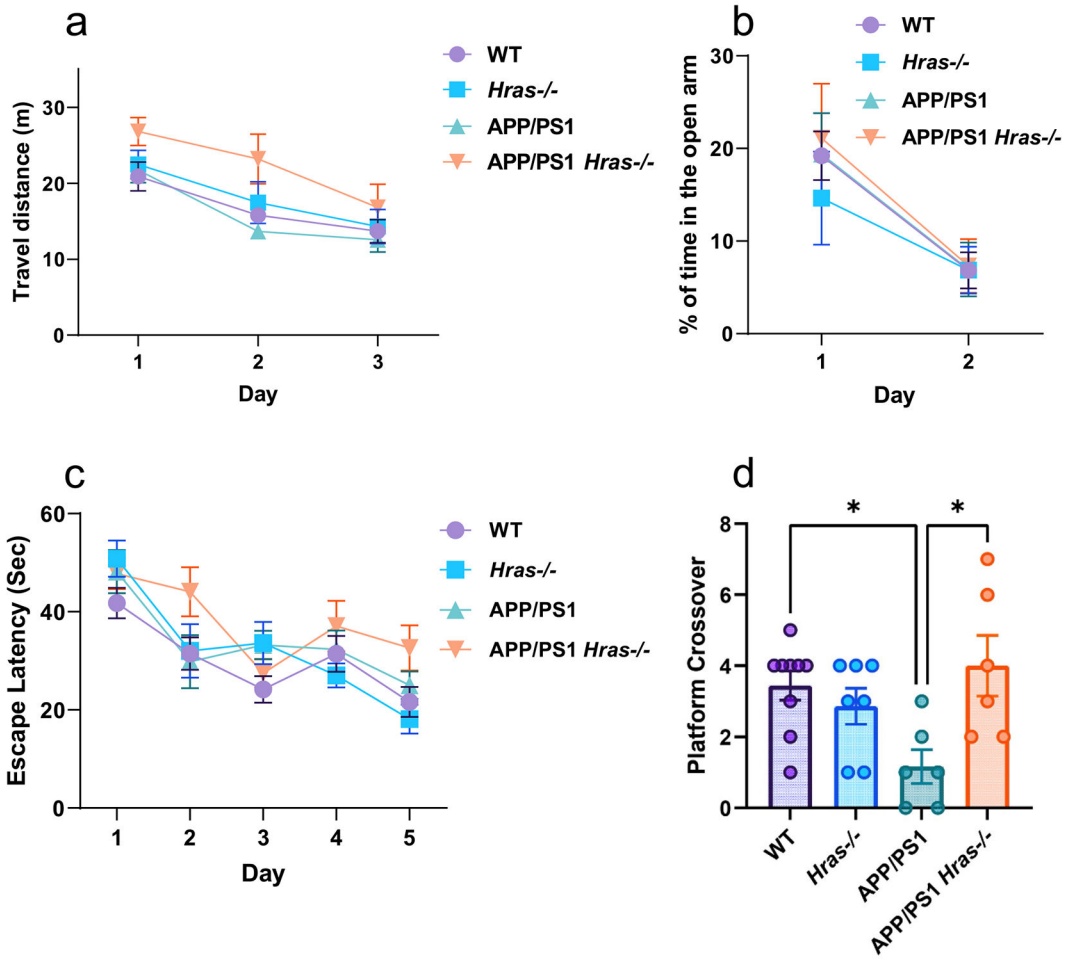

Fig. 1.

Hras deletion rescues spatial memory retention deficits in APP/PS1 mice. Nine-month-old WT, *Hras−/−*, APP/PS1, and APP/PS1 *Hras−/−* littermates (n = 6–9 mice/genotype) were examined for locomotive function in the open-field test (**a**), anxiety levels in the elevated plus-maze test (**b**), and spatial learning and memory in the Morris water maze test (**c, d**). *Hras* deletion did not affect the locomotive function (**a**), anxiety levels (**b**), and learning capacities during the acquisition phase (**c**). APP/PS1 mice showed memory retention deficits during the probe trial compared with WT, and importantly, APP/PS1 *Hras−/−* performed significantly better than APP/PS1 mice and restored to a similar level of performance as WT mice (**d**; *$p < 0.05$, one-way ANOVA followed by Tukey's HSD post hoc test)

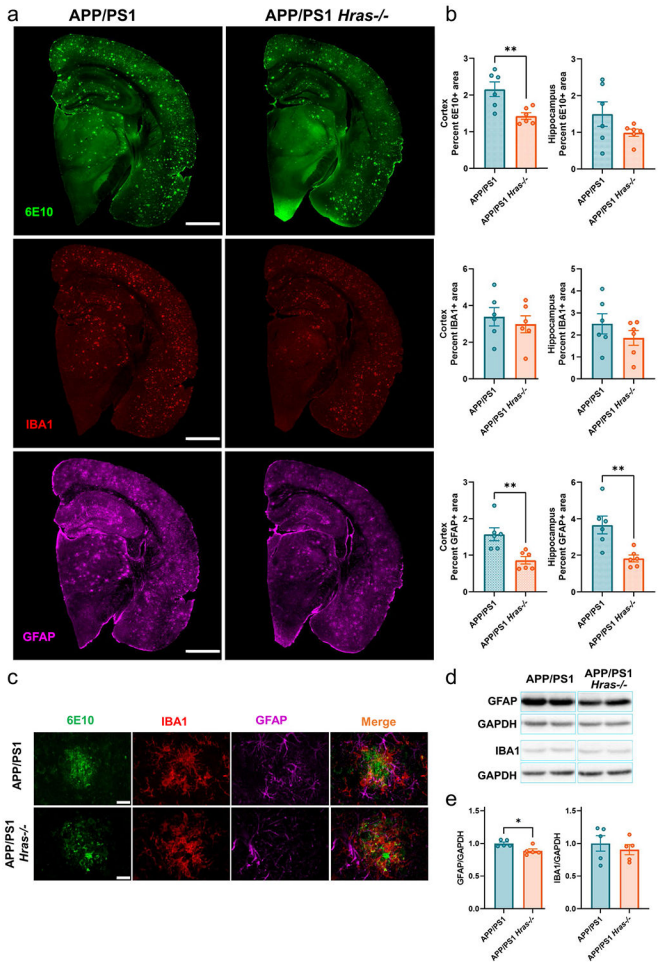

Fig. 2.

Hras deletion reduces cortical amyloid deposition and astrogliosis. Representative stitched brain images (**a**) of triple immunofluorescent labeling of amyloid plaques by 6E10, microglia by IBA1, and astrocytes by GFAP and quantifications (**b**) of percentage area stained in the hippocampus and cortex. Compared with APP/PS1, APP/PS1 *Hras*−/− mice showed reduced cortical amyloid deposition and alleviated astrogliosis in both cortex and hippocampus but no change in microglosis (** $p < 0.01$, Student's *t*-test). Four sections per animal were analyzed and averaged. Representative plaque images (**c**) under 100x objective in the cortex of APP/PS1 and APP/PS1 *Hras*−/− mice. Western blots (**d**) and their quantifications (**e**) showed significantly reduced GFAP expression but not IBA1 expression in the cortex of APP/PS1 *Hras*−/− mice (* $p < 0.05$, Student's *t*-test; $n = 5$–6 mice/genotype). Scale bars: 1 mm in **a** and 20 μm in **c**

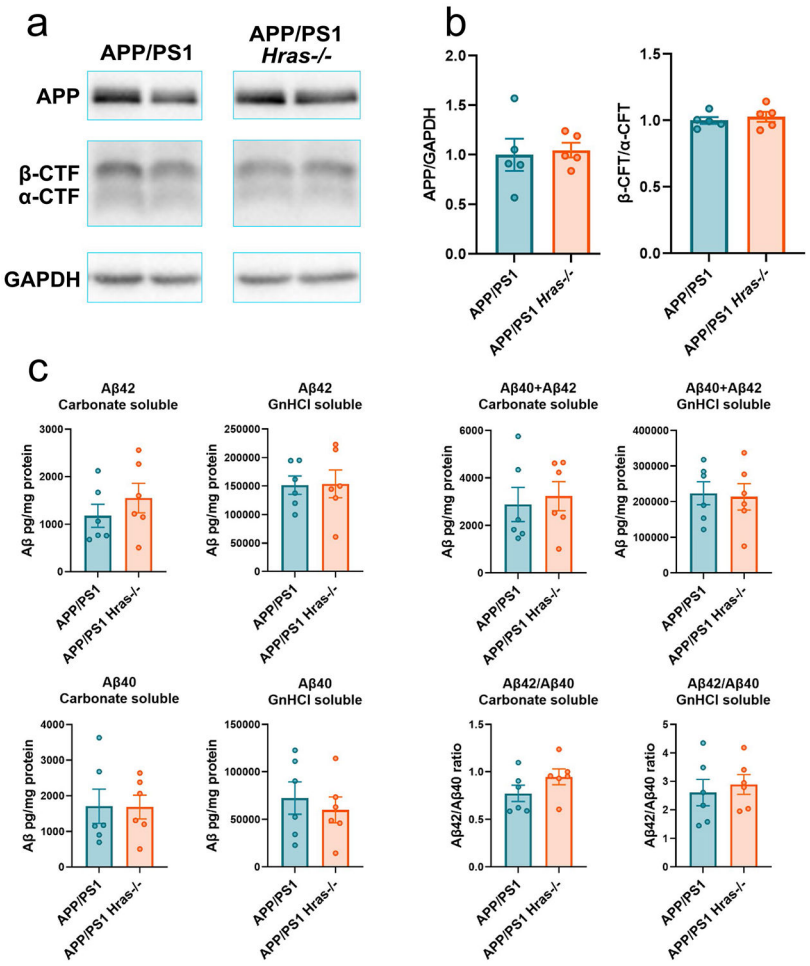

Fig. 3.

Hras deletion does not affect APP expression and processing or overall Aβ levels. Western blot representative images (**a**) and quantification (**b**) showed that no significant differences in the overall expression of APP or its amyloidogenic and non-amyloidogenic cleavage products measured by the ratio of β-CTF/α-CTF between APP/PS1 *Hras*−/− and APP/PS1 mice (n = 5/genotype). $A\beta_{42}$ and $A\beta_{40}$ ELISA (**c**) showed that neither carbonate-soluble nor insoluble (GnHCl-soluble) fractions of $A\beta_{40}$ or $A\beta_{42}$ levels, the total $A\beta_{40}$ and $A\beta_{42}$ levels, nor the $A\beta_{42}/A\beta_{40}$ ratios were altered in the cortical lysate of APP/PS1 *Hras*−/− mice compared with APP/PS1 mice (n=6/genotype)

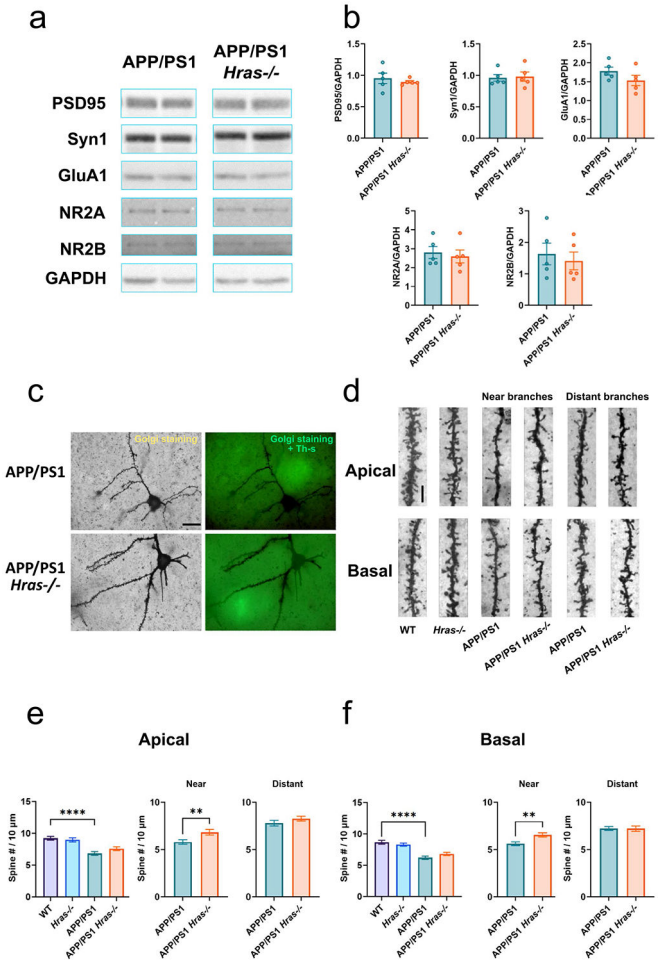

Fig. 4.

Hras deletion protects against dendritic spine loss near amyloid plaques without changing overall spine density or synaptic protein expression. Representative western blot images (**a**) and quantifications (**b**) of synaptic makers in isolated synaptosomes showed similar expression of glutamatergic synaptic makers, including PSD95, Syn1, GluA1, NR2A, and NR2B, in APP/PS1 *Hras*−/− mice compared with APP/PS1 mice ($n = 5$ mice/genotype). Representative Golgi-Cox impregnation combined with Th-S co-staining (**c**) identified dendritic branches in the approximation of plaques. Representative images of dendritic branches (**d**) and quantifications of apical (**e**) and basal (**f**) dendritic spine density revealed that *Hras* deletion protected dendritic spines from Aβ toxicity and reduced spine loss near amyloid plaques. ($n = 50$–70 branches/4 mice/genotype; $^{**}p < 0.01$, $^{****}p < 0.0001$, Student's *t*-test). Scale bars: 20 µm in **c** and 5 µm in **d**

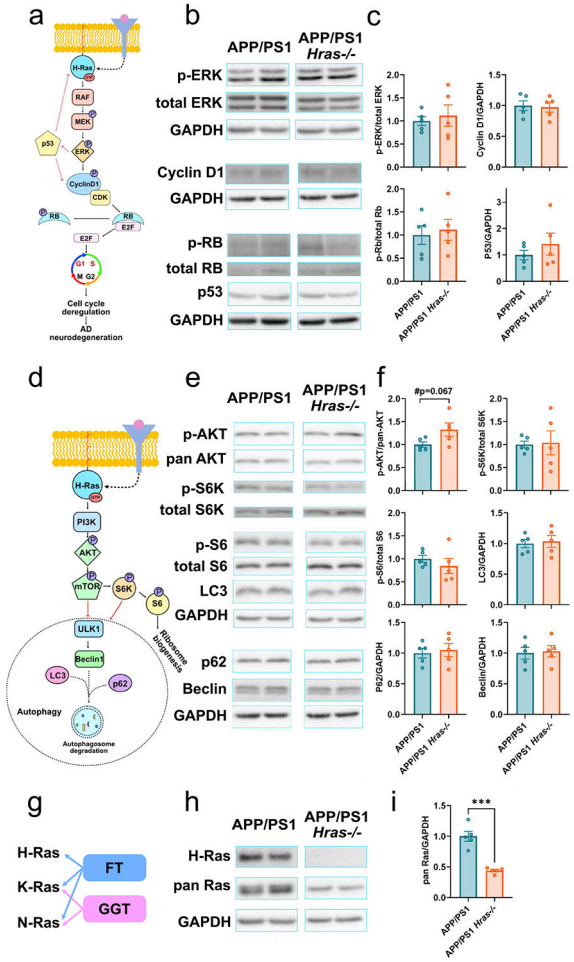

Fig. 5.

Hras deletion does not affect the MAPK/ERK or the PI3K/AKT pathway. H-Ras-MAPK/ERK pathway (**a**). H-Ras activation leads to the ERK signaling cascade that regulates the cell cycle, which can contribute to neurodegeneration in AD. Representative western blot images (**b**) and quantifications (**c**) of key molecules in the H-Ras-MAPK/ERK pathway showed comparable ERK pathway activation in APP/PS1 and APP/PS1 *Hras*−/− mice. H-Ras-PI3K/AKT signaling pathway (**d**) leads to the activation of mTOR and regulation of autophagy. Representative western blot images (**e**) and quantifications (**f**) showed a trend of increase in p-AKT but no changes in other key molecules in the PI3K/AKT pathway in APP/PS1 *Hras*−/− mice compared with APP/PS1 controls. H-Ras is exclusively prenylated by FT and K-Ras and N-Ras are isoforms of H-Ras that can be prenylated by both FT and GGT (**g**). Representative western blot images (**h**) and quantifications (**i**) showed that H-Ras protein was absent in the APP/PS1 *Hras*−/− mice. Without H-Ras, the total Ras level (pan-Ras) in the brain decreased by 50%, and thus K-Ras and N-Ras were not overexpressed to compensate for the loss of H-Ras. The reduced pan-Ras level appeared to be sufficient to drive the activation of ERK/MAPK and the PI3K/AKT pathway (***$p < 0.001$, Student's *t*-test, $n = 5$ mice/genotype)

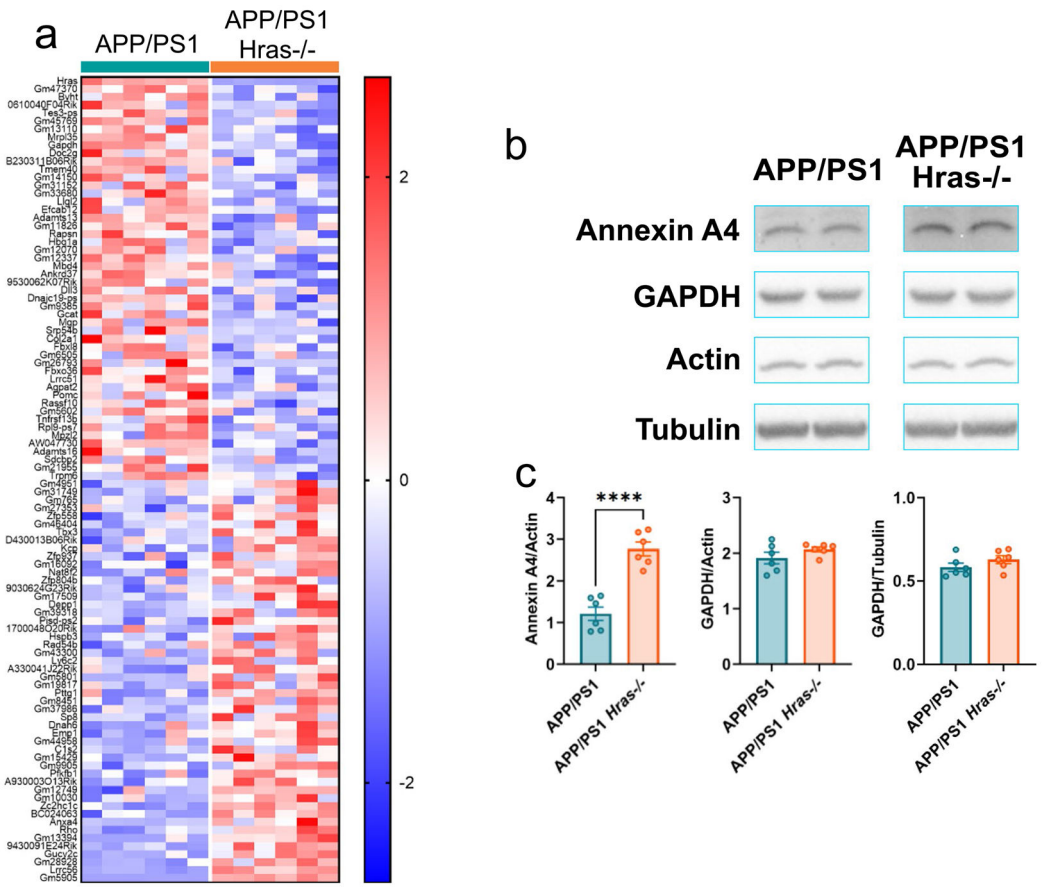

Fig. 6.

Ablation of *Hras* modifies the expression of select genes including *Anxa4*. Heatmap of RNA-Seq expression z-scores (**a**) for the top 100 most variable genes in APP/PS1 and APP/PS1 *Hras−/−* mice. Western blotting representative images (**b**) and quantifications (**c**) showed comparable GAPDH protein expression levels between genotypes either normalized to Actin or Tubulin and confirmed the upregulation of ANXA4 at the protein level in APP/PS1 *Hras−/−* mice (**** $p < 0.0001$, Student's *t*-test, $n = 6$ mice/genotype)

Table 1

Differentially expressed genes (DEGs) in APP/PS1 *Hras−/−* compared with APP/PS1 mice

Gene name	Up/down regulation	Log2 fold change	Adjusted *p*-value	Function	References
Gm5905	Up	6.71	5.69E–182	Ribosomal protein S9 predicted gene	[36]
Lrrc56	Up	0.91	3.97E–11	Cell projection organization	[36, 37]
Anxa4	Up	1.06	0.001	Plasma membrane repair, calcium homeostasis, inhibition of NF-κB signaling, inhibition of interleukin-8 production	[34-36]
Gm13394	Up	4.61	0.028	Glyceraldehyde-3-phosphate dehydrogenase pseudogene	[36]
Gucy2c	Up	2.08	0.033	Protein binding, kinase activity regulation, guanylate cyclase activity, maintaining gut-brain endocrine homeostasis	[36, 38]
Smim10l1	Up	0.22	0.067	Catalytic activity	[36]
Hras	Down	−1.95	2.45E–114	Oncogene, GTPase (targeted deletion)	[6]
Gapdh	Down	−0.51	0.001	Energy metabolism and ATP production, cellular aging and apoptosis	[39, 40]
Mbd4	Down	−0.52	0.065	Catalytic activity, hydrolase activity, DNA repair, and methylation	[41]
Mrpl35	Down	−0.51	0.070	Mitochondrial translation and metabolism	[42]